43rd Aerospace Sciences Meeting, January 10-13,2005, Reno,NV

Aerodynamics and Flight Control of Flapping Wing Flight Vehicles: A Preliminary Computational Study

Sriram*, Arathi Gopinath†, Edwin van der Weide‡
Claire Tomlin§and Antony Jameson¶
Department of Aeronautics and Astronautics
Stanford University, Stanford, CA 94305-3030

I. Introduction

The dexterity and gracefulness of winged creatures have captured the imagination of humans for a long time. Insects have evolved sophisticated flight control mechanisms that permit a remarkable range of maneuvers. To replicate the flight behavior of insects it is first necessary to obtain a good understanding of the kinematics of insect flight and the physics of the fluid flow around the body of the insects. This in turn might allow for the identification of efficient aerodynamic shapes and control mechanisms that can be replicated in unmanned robotic vehicles.[9] These robotic vehicles can then be used to perform tasks that are not possible with conventional fixed wing or rotary flight vehicles. If one agrees that insects have highly optimized wing shapes and control mechanisms, then a study into the flight control of insects can also be used to validate optimization techniques that recover the optimal wing shape, pitching frequency, stroke amplitude and other control inputs.

Insect flight control has been studied extensively from a physiological perspective, but its mechanics are less well known. Even when the kinematic changes elicited by a given stimulus have been defined, their consequences for aerodynamic force production often remain obscure. Quasi-steady aerodynamics has been largely supplanted by unsteady theories and is widely accepted as the mechanism that leads to the forces produced by insects in flight.[3,4] Lighthill[1] performed some of the earliest theoretical studies on the aerodynamics of insect flight and Weis-Fogh and Jensen[2] determined the variation of the positional angle of fore and hind wings during flight of Schistocerca gregaria. A variety of experimental studies has enabled a better understanding of the nature of wing articulation by insects in hover and forward flight.[5,6,7] While these studies enabled the authors to propose a possible theory for insect flight, the lack of a complete understanding of the flight control mechanisms has prevented a more comprehensive understanding of insect flight control. It is not clear how many degrees of freedom an insect controls to enable it to perform its various maneuvers. Further, insects in controlled laboratory environments tend to produce lift and drag forces that are different from those observed in nature, leading one to look for alternate analysis tools. It is also difficult to replicate subtle shifts in the center of gravity or even get a good estimate of the center of gravity of the insect and this further clouds our understanding. Finally, there is a wide body of evidence that suggests that unlike conventional aircraft/flight vehicles, the control inputs are typically the pitching frequency, the stroke amplitude, the change in angle of attack during the pitching cycle and the twist in the wing. Each of these control inputs produce coupled motions in roll, yaw and pitch motion and this non-orthogonal nature of the response to the control inputs complicates the process of using separate control inputs to generate specific maneuvers. The ability of insects to devise control inputs for particular manouvers is interesting

*Research Associate, Stanford University
†Doctoral Candidate, Stanford University
‡Research Associate, Stanford University
§Associate Professor, Stanford University
¶Professor, Stanford University

Copyright © 2005 by the American Institute of Aeronautics and Astronautics, Inc. The U.S. Government has a royalty-free license to exercise all rights under the copyright claimed herein for Governmental purposes. All other rights are reserved by the copyright owner.

from a practical and theoretical viewpoint as it might provide us with clues to develop more efficient control mechanisms for conventional aircraft.

The purpose of this paper is to take a first step towards simulating and understanding the flight behavior of insects. To achieve this objective, in this paper we study the characteristics of flapping wings. Our contributions are two fold. On the one hand we use a recently developed computational tool to obtain estimates of time-averaged lift and drag for time-periodic flows. Using this tool, we obtain estimates of the forces for varying flapping frequencies and angular amplitudes. The other is on the control theory front, where we use numerical methods to solve the Hamilton-Jacobi (HJ) equations that provide us with estimates of the optimal trajectories and control inputs. Knowledge of the force maps and the control inputs enables us to determine the flapping frequency and the angular amplitudes required to perform particular maneuvers.

II. Computational Model used in this study

The computational model in this study uses a two dimensional cambered flat-plate to represent a wing section. For this wing shape we first determine the forces generated by the flapping motion. The forces are determined by numerically solving the unsteady laminar Navier-Stokes (NS) equations over a time period equal to the period of the pitching cycle. Using this computational tool, we obtain estimates of the forces for various frequencies and stroke amplitudes. This provides us with a map of the forces produced by the flapping motion.

To model the flight of the vehicle we then use a dynamical model for the insect/vehicle. This model uses ordinary differential equations to govern the evolution of the planar position and the heading angle. The control input for this model is the turning force that results in a change in the heading angle. This is to be realized by differentially pitching (frequency and/or stroke amplitude) the wing on either side of the body. The force maps provided by the numerical solution to the NS equations give us a bound on the maximum and minimum turning force we can generate. Hence, we now have a simplified model for the motion of the vehicle.

To determine the optimal control inputs we associate a performance measure to the above dynamical model and formulate Hamilton-Jacobi (HJ) equations that govern the evolution of the performance measure. In particular, we use two performance measures, the first one is the terminal distance from a circle centered around the origin and the second is the time to reach this circle. For the first performance measure, we solve the time-dependent HJ equations to determine the possible positions that can lead the vehicle to the circle. For the second performance measure, we solve the static HJ equations to determine the optimal trajectories and the control inputs along the trajectory.
An overview of the computational process is shown in Figure 1.

III. Fast and Efficient Numerical Solution Techniques

To obtain accurate and fast estimates of the forces produced during the flapping motion, one needs to efficiently integrate the Navier-Stokes equations in time. The dual time stepping scheme[12] provides a convenient formulation for a fully implicit scheme for truly unsteady flows. To exploit the periodic nature of the flow over insect wings, alternate numerical techniques can be used. Recently Gopinath and Jameson[13] have developed a time spectral method to analyze periodic unsteady flows. This method provides substantial savings in computational time as the flow solution can be obtained with a small number of spectral modes, and also eliminates the need to integrate the governing equations over a few pitching cycles. The combined effect of these methods is to provide reductions in computational times of the order of 10 over the dual time stepping scheme.

1. Time-Spectral Methods

Taking advantage of the periodic nature of the problem, a Fourier representation in time can make it possible to achieve spectral accuracy.
The semi-discrete form of the governing equations can be written as,

$$V\frac{\partial w}{\partial t} + R(w) = 0.$$

where V is the volume/area of each computational cell and w is the vector of conservative variables, $\{\rho, \rho u, \rho v, \rho E\}$.
The discrete Fourier transform of w is given by

$$\hat{w}_k = \frac{1}{N} \sum_{n=0}^{N-1} w^n e^{-ik\frac{2\pi}{T}n\Delta t}$$

and its inverse transform by,

$$w^n = \sum_{k=-\frac{N}{2}}^{\frac{N}{2}-1} \hat{w}_k e^{ik\frac{2\pi}{T}n\Delta t}, \tag{1}$$

where the time period T is divided into N time steps, $\Delta t = T/N$.
Then, we discretize the governing equations as a pseudo-spectral scheme,

$$VD_t w^n + R(w^n) = 0. \tag{2}$$

McMullen et.al.[10,11] solved the time accurate equations in (2) by transforming them into the frequency domain and introducing a pseudo-time t^*,

$$V\frac{\partial \hat{w}_k}{\partial t^*} + Vik\frac{2\pi}{T}\hat{w}_k + \hat{R}_k = 0.$$

Alternatively, the Global Space-Time Multigrid Spectral Algorithm[13] proposes to solve the governing equations in the time-domain, considerably gaining on the computational time required to transform back and forth to the frequency domain.
From Eq.(1), the result of applying the time discretization operator D_t can be written as

$$D_t w^n = \sum_{k=-\frac{N}{2}}^{\frac{N}{2}-1} ik\frac{2\pi}{T}\hat{w}_k e^{iknt\Delta t}.$$

This summation involving the Fourier modes $\hat{w}_k$, can be rewritten in terms of the conservative variables w in the time domain as

$$D_t w^n = \sum_{m=-\frac{N}{2}+1}^{\frac{N}{2}-1} d_m w^{n+m},$$

where

$$d_m = \begin{cases} \frac{2\pi}{T}\frac{1}{2}(-1)^{m+1}cot(\frac{\pi m}{N}) & : \quad m \neq 0 \\ 0 & : \quad m = 0 \end{cases}$$

Note that $d_{-m} = -d_m$. The operator D_t hence is a central difference operator connecting all the time levels, so yielding an integrated space-time formulation which requires the simultaneous solution of the equations for all time levels.

A pseudo-time t^* is introduced in an approach similar to the the dual time stepping algorithm, and the equations are time marched to a periodic steady-state

$$V\frac{\partial w^n}{\partial t^*} + VD_t w^n + R(w^n) = 0.$$

This method was validated for a pitching airfoil in transonic flow and the comparisons with experimental data are shown in Gopinath and Jameson.[13]

2. Force Predictions

Using the time-spectral method we obtain estimates of the forces for a range of flapping frequencies and angular amplitudes. The calculations are performed on a two dimensional section with 3 percent camber and the computational meshes are shown in Figures 2 and 3. The computational grids have an H-mesh topology and a two block structure. Each block has 224 points in the flow direction and 64 points in the directional

normal to the wing section. The points in the normal direction are stretched in a geometric ratio and there are about 18 points within the boundary layer. The computations assuming laminar flow at a Reynolds number of 5000. The flow computations were performed using 3 levels of multigrid to accelerate convergence along with second-order spatial discretizations and multi-step modified Runge-Kutta time integration schemes. Figure 4 shows a typical convergence history for the calculations. Figures 5 and 6 show the unsteady lift and drag coefficients over one pitching cycle for various time intervals and it was observed that 8 time intervals were enough to obtain converged estimates of the unsteady lift and drag. Figure 7 shows the non-dimensional pressure distribution at four instances during the pitch cycle. The wing section was pitched according to a sinusoidal wave form with an amplitude, a, and a frequency ω. Figures 8 and 9 show the time-averaged lift and drag for various reduced frequencies and angular amplitudes where the reduced frequency is defined for a chord, c, and free-stream velocity of V_{inf} as

$$\omega_r = \frac{\omega c}{2 * V_{\text{inf}}}$$

The value of time-averaged C_d shows that for the pitching frequencies and the angular amplitudes we considered, the flapping motion of the wing section produces negative thrust. This means that we can produce a turning force by differentially pitching the wing section on either side of the body. Using this knowledge and assuming that the maximum turning force is a fraction of the forward velocity, in the next section we devise control laws to determine the optimal control inputs and trajectories. In addition, if the pitching time is small in comparison to the flight time, we can use time-averaged values of the lift and drag to determine the control inputs during flight.

IV. Flight Control through Hamilton-Jacobi Equations

Using estimates of the forces produced by the flapping motion one can devise an approximate dynamical model for the insect. Associating a performance measure with the system we can then determine the optimal control inputs that lead to an improvement in the performance measure. In this study we assume the motion of the insect occurs in a plane and the control inputs are the flapping frequency and the angular amplitude. By varying the control inputs on either side of the body we can generate a turning force. As the yaw and roll motions are coupled, this approach is a first approximation that ignores the associated roll motion caused by the control inputs. Finally, we consider two performance measures, one in which we wish to minimize our distance from a target and the other in which we wish to enter a target set in minimum time.

The dynamical equations for motion in a plane can be written as

$$\frac{dx}{dt} = V cos(\phi); \quad \frac{dy}{dt} = V sin(\phi); \quad \frac{d\phi}{dt} = \sigma \qquad V = 1; \; \sigma = 0.1 \tag{3}$$

where V is the velocity of the vehicle, and σ is the control input that is chosen to minimize a particular cost function. Let the cost function be written as

$$J = L(x(T)) + \int_0^T G(x, u)dt$$

The HJ equations for the cost-to-go,V, can be written as

$$\frac{\partial V}{\partial t} + min_u H(\nabla V, u, x) = 0 \qquad V(T) = L(x(T)) \tag{4}$$

In the following sections we present results from two different cost functions.

A. Reach Sets

Using knowledge of the forces generated by the flapping motion of the wing, we use the HJ formulation to determine the states that can lead us to a circle of a particular radius. The computation of the reach

set was initially performed by Mitchell, Bayen and Tomlin[18] for differential game problems and shown to be an efficient technique to recover the possible states that can lead to a terminal condition for non-linear dynamical systems. We use the same computational technique to solve the HJ equations associated with the dynamics of the vehicle. The HJ equations are solved using a fifth-order WENO spatial discretization[20] and a third order order TVD Runge-Kutta time integration scheme.

For problems in which the minimizing control inputs can be obtained in functional form, the equations reduce to a PDE with time derivatives and space-derivatives. WENO schemes have been shown to be efficient to approximate the spatial derivatives of the value function especially for problems with discontinuous value functions. TVD Runge-Kutta schemes provide stable and consistent approximations to the time derivative.

In the HJ equations, the spatial derivatives appear in the Hamiltonian and hence we write a local Lax-Freidrichs approximation for the Hamiltonian as

$$\begin{aligned} \nabla\hat{V} &= \frac{\nabla V^+ + \nabla V^-}{2} \\ \hat{H}(\nabla V, x) &= H(\nabla\hat{V}, x) - \sigma_x \frac{\nabla\hat{V}^+ - \nabla\hat{V}^-}{2} \\ \sigma_{x_j} &= max_{j-s<j<j+s} \frac{\partial H}{\partial \nabla V} \end{aligned} \tag{5}$$

where $2s$ is the width of the stencil used to approximate the gradients of V. As the fifth order scheme uses a 5 point stencil centered around each grid point to compute the derivatives, near the edges of the discrete state-space, we use a one-dimensional quadratic approximation to update the value function. This approximation locally reduces the accuracy of the method to second order but our simulations show that it does not affect the values in the interior of the computational space.

Using the above approximation for the spatial terms in the HJ equation, a TVD Runge-Kutta scheme can be used to integrate the system of semi-discrete equations in time. The explicit nature of the time integration scheme restricts the maximum allowable time-step of the approximation scheme. A third-order accurate TVD Runge-Kutta scheme that integrates the state from n to $n+1$ can be written as

$$\begin{aligned} V^1 &= V^n + \Delta t\hat{H}(V^n) \\ V^2 &= \frac{3}{4}V^n + \frac{1}{4}V^1 + \frac{1}{4}\Delta t\hat{H}(V^1) \\ V^{n+1} &= \frac{1}{3}V^n + \frac{2}{3}V^2 + \frac{1}{3}\Delta t\hat{H}(V^2) \end{aligned} \tag{6}$$

$$\tag{7}$$

Figure 11 shows the result of a time dependent evolution of the terminal state after a period of 2 time units. The terminal state is a cylinder with a radius of 5 units. The surface shown in the figure represents the regions in state-space that can evolve into the terminal state. As can be seen from the figure, there are certain headings from which it is not possible to evolve into the terminal state in the given time. In practice, we would like to determine the flapping motions that increase the extent of the reach set so that we can reach a desired terminal state in a given time.

B. Minimum Exit Time

As we are also interested in computing the optimal control inputs along trajectories that lead us to the terminal circle, we use an alternate performance measure, the minimum-time-to-reach and solve the associated static Hamilton Jacobi equation to recover the optimal trajectories. The HJ equations are solved using a method proposed by Kao, Osher and Qian[16] that employs repeated Gauss-Seidel sweeps to improve an initial guess for the time to reach function.

Let Ω represent the portion of state-space in which the dynamics evolves and T represent the target set that the model would like to reach in minimum time. The HJ equations can be written as

$$\begin{aligned} H(x, \nabla V) &= R \quad in \quad \Omega \\ V &= 0 \quad on \quad T \end{aligned}$$

To construct an approximation scheme, the Lax-Friedrichs Hamiltonian, H_{lf}, can be written in one dimension as

$$H_{lf} = H\left(x, \frac{V^+ + V^-}{2}\right) - \sigma_x \left(\frac{V^+ - V^-}{2}\right)$$

where σ_x is the artificial viscosity term modeled as $max\|\frac{\partial H}{\partial \nabla V}\|$. Using forward and backward difference operators to approximate the gradients V^+ and V^-, $H_{lf} = R$ can be written as

$$H\left(x, \frac{V_{i+1} - V_{i-1}}{2\Delta x}\right) - \sigma_x \left(\frac{V_{i-1} - 2V_i + V_{i+1}}{2\Delta x}\right) = R$$

where V_i is the approximation for the value at the discrete grid point i. The above equation can be rewritten for the unknown value function at each point in discrete state-space in a form that is easy to use in a Gauss-Seidel algorithm as

$$V_i = \frac{\Delta x}{\sigma_x}\left(R - H(x, \frac{V_{i+1} - V_{i-1}}{2\Delta x})\right) + \frac{V_{i+1} + V_{i-1}}{2}$$

Using an initial guess for V that satisfies the boundary condition on the target set, the above approximation for V_i can be used to iteratively improve the initial guess until the discretized HJ equations are satisfied (within numerical accuracy) everywhere in state-space. Kao, Osher and Qian[16] also suggest boundary conditions for approximations at the edge of the discrete state-space.

Figures 12,13 and 14 show plots of the time to reach function for three heading angles. These computations were performed on a discretization of state-space that used 150 equally spaced points in each state and used 50 Gauss Seidel sweeps to improve an initial guess for the value function.

Figure 15 shows the projections of the optimal trajectories on the (x, y) plane for initial heading angles of 240 degrees. It can be seen that the optimal trajectories are approximately straight lines as one would expect. For some initial positions the geodesic with minimum length is a curved path and nature of the geodesic depends on the maximum turning force, σ.

C. Conclusions and Future Work

In this study we have taken a first step to integrate the aerodynamic and control theoretical algorithms to study the characteristics of flapping wing-sections. The use of fast and efficient numerical methods to solve the partial differential equations governing fluid flow and optimal control problems provides us with a convenient frame-work to provide both force and control input estimates.

In the future we plan to extend this approach to refine the aerodynamic and control computations. The envelope of frequencies and angular amplitudes for the aerodynamic computations needs to expanded and incompressible computations need to be performed to make the predictions more realistic. On the flight control side, a six degree of freedom model needs to be used instead of the simplistic planar model used in this study. The combination of these two refinements will enable us make quantitative statements about the flight behavior of insects that can then be exploited in engineering designs. Further, by estimating the control authority required to achieve particular maneuvers, we can then use an adjoint based approach to determine optimal shapes and control mechanisms like flapping frequency, amplitude of flapping, wing twist etc. that will provide a design tool for small-scale flight vehicles.

V. Acknowledgements

The authors would like to thank Sangho Kim, Stanford University, for generating the initial computational meshes for the numerical simulation of the flapping wing sections.

References

[1]Lighthill, J. Mathematical Biofluidynamics, Regional Conference Series in Applied Mathematics, SIAM, 1975.

[2]Weis-Fogh T. and Jensen M. Proceedings of the Royal Soceity B. 239, pp. 415-584, 1956.

[3]Ellington, C.P., Van Der Berg C, Willmott, A.P. and Thomas, A.L.R. Leading-edge vortices in insect flight, Nature, 384, 626-630, 1996.

[4]Dickinson, M.H., Lehmann, F., Sane, S.P. Wing Rotation and the Aerodynamics basis of insect flight, Science, 284, pp. 1954-1960, 1999.

[5]Ellington, C.P. The aerodynamics of hovering insect flight, Philosophical Transactions of Royal Society of London, B, 305, 1-181, 1984.

[6]Willmott, A.P., Ellington, C.P. and Thomas, A.L.R., Flow visualization and unsteady aerodynamics in the flight of the hawkmoth, Manduca sexta Philosophical Transactions of the Royal Society of London, B, 352, 303-316, 1997.

[7]Wang, Z.J., Birch J.M. and Dickinson M.H., Unsteady forces and flow in low Reynolds number hovering flight: two dimensional computations vs. robotic wing experiments Journal of Experimental Biology 207, 449-460, 2004.

[8]Jones, K, Castro B.M, Mahmoud O, and Platzer M, Numerical and Experimental Investigation of Flapping Wing Propulsion in Ground Effect, AIAA Paper 2002-0866, Aerospace Sciences Meeting, Reno, NV, 2002.

[9]J. Yan and R.S. Fearing, Wing Force Map Characterization and Simulation for the MicroMechanical Flying Robotic Insect, IEEE Int. Conf. on Intelligent Robots and Systems, Oct 28-30, 2003, Las Vegas NV.

[10]M. McMullen, A. Jameson and J.J. Alonso, Acceleration of Convergence to a Periodic Steady State in Turbomachinery Flows AIAA 39th Aerospace Sciences Meeting, 01-0152, Reno, NV, 2001.

[11]M. McMullen, A. Jameson and J.J. Alonso, Application of a Non-Linear Frequency Domain Solver to the Euler and Navier-Stokes Equations AIAA 40th Aerospace Sciences Meeting and Exhibit, 02-0120, Reno, NV, 2002.

[12]A. Jameson. Time dependent calculations using multigrid, with applications to unsteady flows past airfoils and wings. *AIAA paper 91-1596*, AIAA 10th Computational Fluid Dynamics Conference, Honolulu, Hawaii, June 1991.

[13]A. Gopinath and A. Jameson, Time Spectral Method for Periodic Unsteady Computations over Two and three Dimensional Bodies AIAA 43th Aerospace Sciences Meeting and Exhibit, 05-1220, Reno, NV, 2005.

[14]A. Jameson. Optimum Aerodynamic Design Using Control Theory, Computational Fluid Dynamics Review 1995, Wiley, 1995.

[15]J. J. Alonso, L. Martinelli, and A. Jameson. Multigrid unsteady Navier-Stokes calculations with aeroelastic applications. *AIAA paper 95-0048*, AIAA 33rd Aerospace Sciences Meeting, Reno, NV, January 1995.

[16]Kao. C.Y., Osher S. and Qian J., Lax Friedrichs sweeping scheme for static Hamilton-Jacobi equations, Journal of Computational Physics, Vol. 196, Issue 1, pp. 367 - 391, 2004.

[17]Liu, X-D, Osher S., Chan T., Weighted essentially non-oscillatory schemes, Journal of Computational Physics, 115, pp. 200-212, 1994.

[18]Mitchell I., Bayen A., Tomlin C., Computing reachable sets for continuous dynamic games using level set methods, to appear in IEEE Transactions on Automatic Control, 2005.

[19]Osher S., A level set formulation for the solution of the Dirichlet problem for Hamilton Jacobi equations, Journal of Mathematical Analysis and Applications, 24, pp. 1145-1152, 1992.

[20]Osher S. and Shu C-W, Higher order essentially non-oscillatory schemes for Hamilton Jacobi equations, Journal of Numerical Analysis, 28, pp. 907-922, 1991.

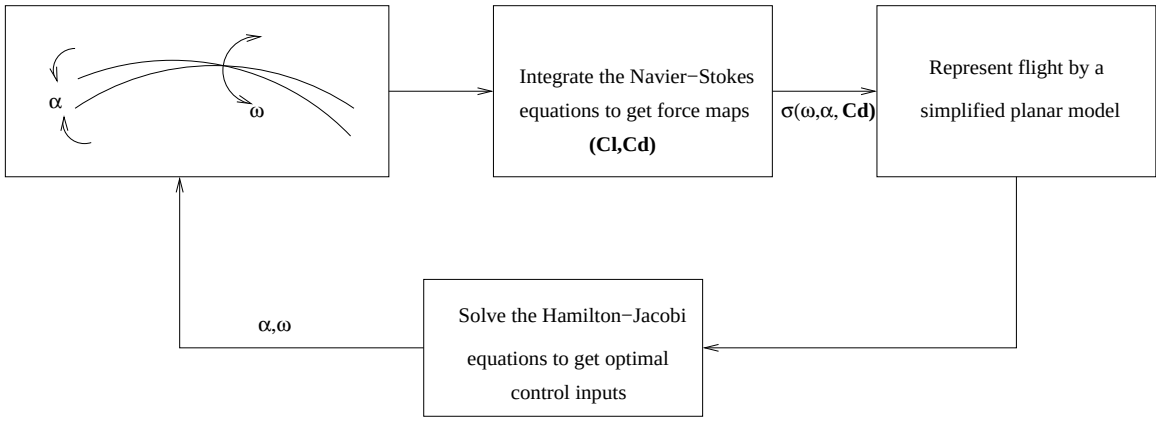

Figure 1. Overview of the computational approach

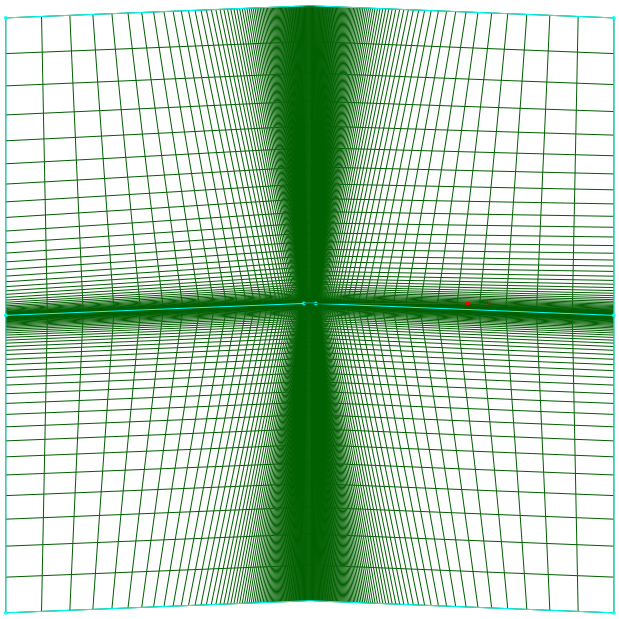

Figure 2. Representative computational grid

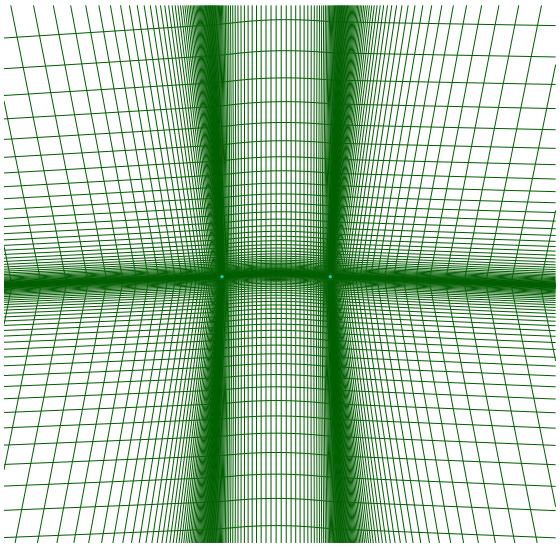

Figure 3. Region of the grid near the wing section

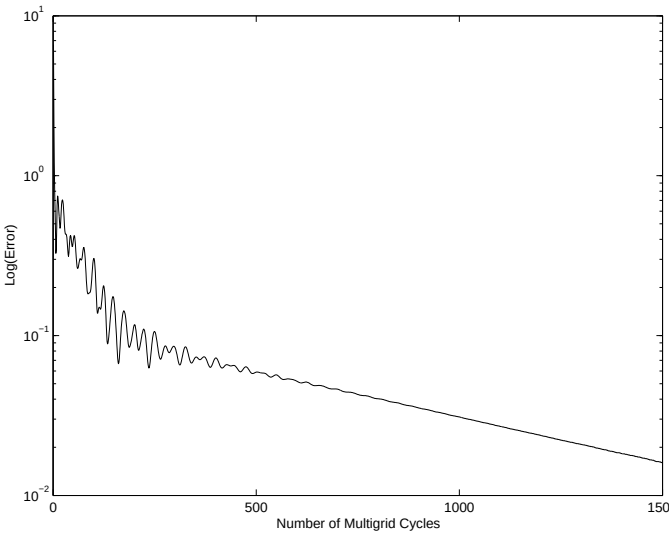

Figure 4. Convergence of RMS of density

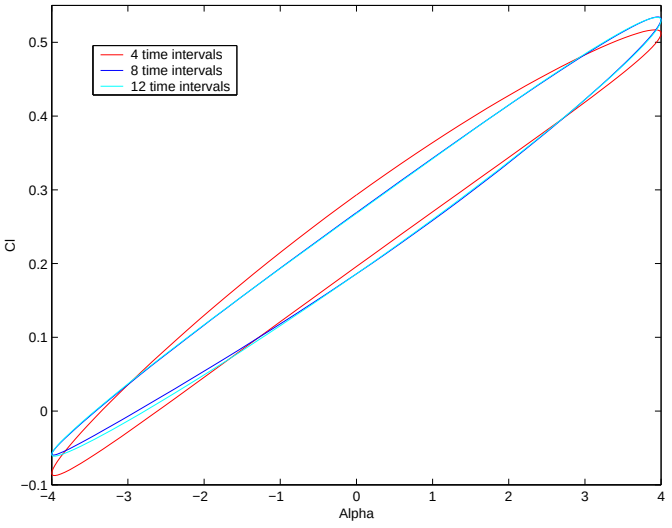

Figure 5. Variation of C_l for a reduced frequency of 0.3 and angular amplitude of 4 degrees

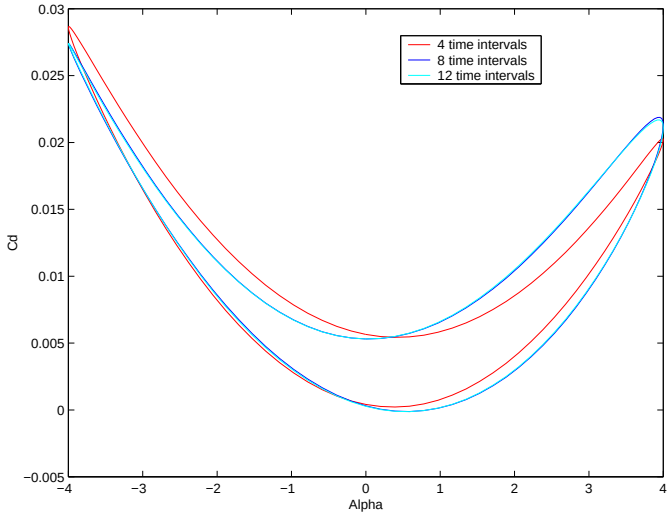

Figure 6. Variation of C_d for a reduced frequency of 0.3 and angular amplitude of 4 degrees

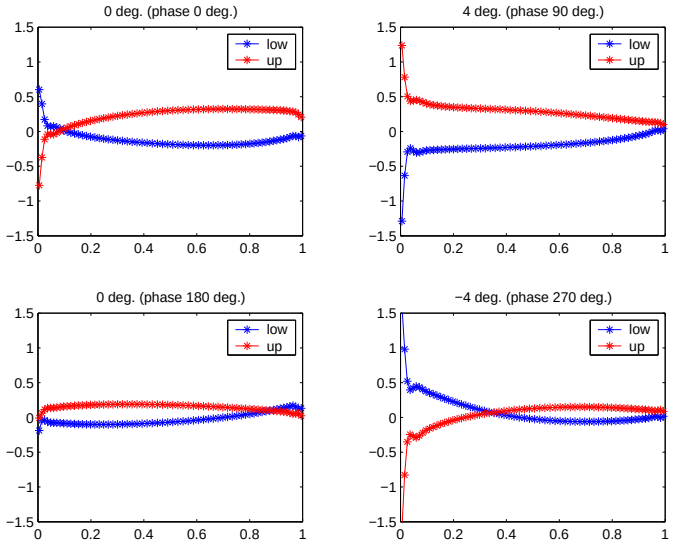

Figure 7. C_p distribution at different instances in the time-period

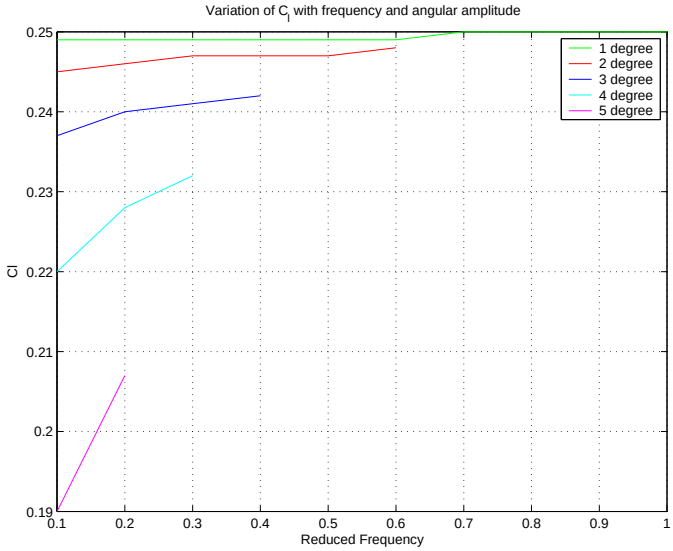

Figure 8. Variation of C_l with reduced frequency and angular amplitude

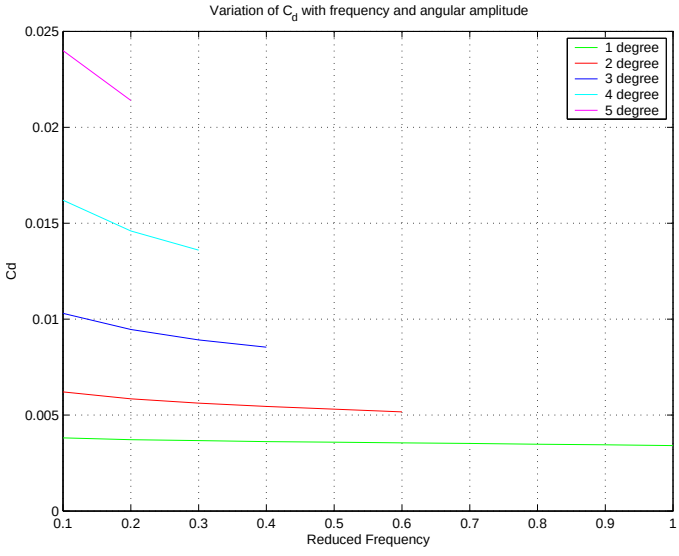

Figure 9. Variation of C_d with reduced frequency and angular amplitude

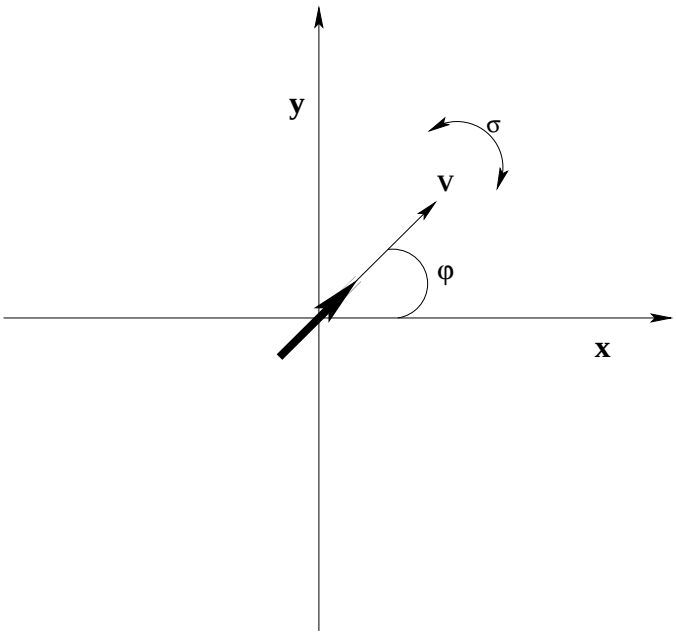

Figure 10. Coordinates and control inputs

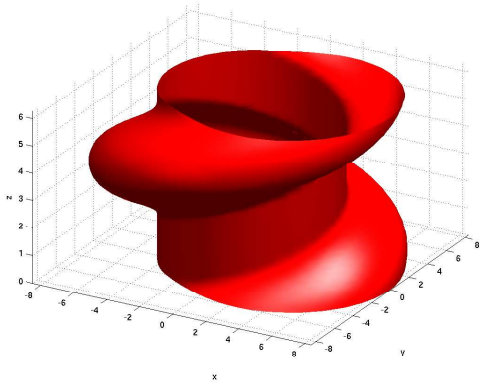

Figure 11. Barrier computed from a time dependent numerical simulation: the region represents the set of initial configurations from which it is possible to reach a circle of radius 5 in time 2 secs. (x,y,z) axes represent (x,y) coordinates of planar position, and z (radians) represents the heading.

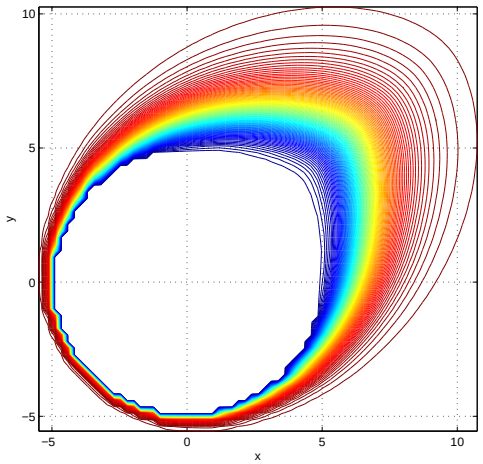

Figure 12. Contours of Time-to-reach function for a heading angle of 225 degrees

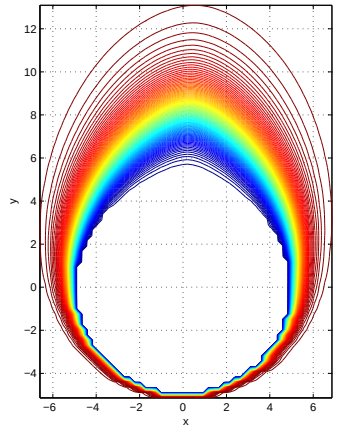

Figure 13. Contours of Time-to-reach function for a heading angle of 270 degrees

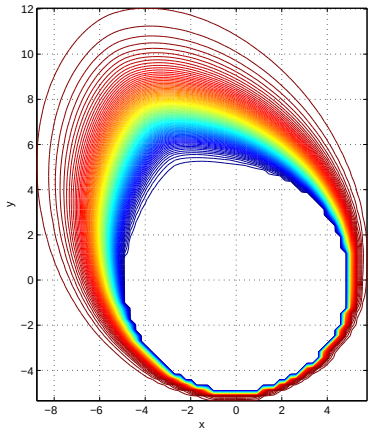

Figure 14. Contours of Time-to-reach function for a heading angle of 300 degrees

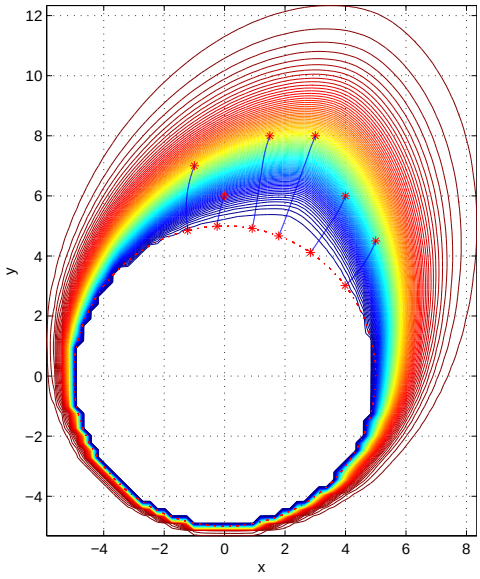

Figure 15. Projections on the (x, y) plane of optimal trajectories for an initial heading angle of 240 degrees